A pore network study of evaporation from the surface of a drying non-hygroscopic porous medium

Alireza Attari Moghaddam, Abdolreza Kharaghani, Evangelos Tsotsas, Marc Prat

A Pore Network Study of Evaporation from the Surface of a Drying Non-Hygroscopic Porous Medium

Alireza Attari Moghaddam, Abdolreza Kharaghani, and Evangelos Tsotsas
Thermal Process Engineering, Otto-von-Guericke University, P.O. 4120, 39106 Magdeburg, Germany

Marc Prat
INPT, UPS, IMFT (Institut de Mécanique des Fluides de Toulouse), Université de Toulouse, Toulouse 31400, France

CNRS, IMFT, Toulouse 31400, France

DOI 10.1002/aic.16004

The phenomena occurring at the surface of a porous medium during drying in the capillary regime are investigated by pore network simulations. The impact of the formation of wet and dry patches at the surface on the drying rate is studied. The simulations indicate an edge effect characterized by a noticeable variation of saturation in a thin layer adjacent to the porous surface. Also, the results indicate a significant nonlocal equilibrium effect at the surface. The simulation results are exploited to test Schlünder's classical model which offers a simple closure relationship between the evaporation rate and the degree of occupancy of the surface by the liquid. In addition to new insights into the surface phenomena, the results open up new prospects for improving the continuum models of the drying process.

Keywords: drying, pore network simulations, coupling with external transfer, non-hygroscopic porous media

Introduction

Drying of porous media has been the subject of scientific publications for at least about a century[1,2] and is still a field of active research.[3] Actually, many aspects of the drying process are not yet well understood, even for the simple situation corresponding to the typical laboratory experiment where water evaporates from a relatively thin capillary porous medium at room temperature. Capillary porous media refer to non-hygroscopic porous media in which adsorption phenomena (bound water) and Kelvin's effect are negligible. They typically correspond to porous media with pore sizes in the micronic range, that is, from about 1 μm to say about 100 μm. As reported for example in Refs. 4 or 5, the drying kinetics of a capillary porous medium can be described in three main periods: namely a first period, the constant rate period (CRP), during which the evaporation rate is constant (or varies only weakly), a second period called the falling rate period (FRP), during which the evaporation rate drops significantly, and a third period called the receding front period (RFP), where evaporation takes place inside the porous medium and not anymore at its surface. In soil physics,[6,7] this description is simplified with the distinction between only two periods: stage 1 and stage 2, where stage 1 corresponds to the CRP and stage 2 corresponds to both the FRP and the RFP.

Correspondence concerning this article should be addressed to M. Prat at mprat@imft.fr or A. Kharaghani at abdolreza.kharaghani@ovgu.de.

This simplification emphasizes the fact that a crucial aspect of the drying process is the transition between the CRP and the FRP (or stage 1/stage 2 transition). From an engineering prospect for instance, maintaining a long CRP can help to minimize the total drying time. The understanding and the prediction of this transition can be considered as one of the remaining fundamental questions in drying of capillary porous media. The classical description of the transition,[4,5,8] essentially takes a porous medium standpoint. This standpoint states that, the CRP/FRP transition occurs when the capillary forces are not sufficient anymore to transport liquid toward the surface at a rate large enough to compensate for the evaporation rate corresponding to the CRP. This is owing to the increasing viscous resistance in the liquid due to progressive decrease in liquid saturation. This is thus essentially a "liquid relative permeability approach" of the transition,[5] as the liquid phase relative permeability decreases with decreasing saturation as the liquid phase connectivity is becoming less and less good. However, one can also look at this transition from the external mass-transfer standpoint. Obviously, the external mass transfer does not "know" what happens inside the porous medium. It only "sees" the surface. Thus, if the evaporation rate decreases this is because the distribution of liquid water at the surface changes, or more precisely the water vapor partial pressure distribution at the entrance of the surface pores. The external mass-transfer standpoint analysis was first developed in Ref. 9 and then in Ref. 10, noting that Schlünder's model[10] has been analyzed and used recently in a series of papers by Or et al. in the context of soil physics,[11,12] and references therein. As recalled later in this article, Schlünder essentially considers

regularly spaced circular liquid pores over a flat surface, where the mass transfer is controlled by diffusion.

However, the surface of a drying porous medium is less simple than considered in Schlünder's model. In addition to "liquid" pores and solid surface, empty pores (i.e., "gas" pores) are also present at the surface. The vapor partial pressure at the entrance of those pores is *a priori* less than the equilibrium vapor pressure prevailing at the entrance of "liquid" pores and not equivalent to a solid surface (where a zero flux condition applies). Also, the liquid distribution changes during drying with the formation of dry and wet patches of evolving size. This suggests that Schlünder's model is probably not sufficient for modeling the impact of changes in pore occupancy at the porous surface on the evaporation rate.

To get insights into this problem, we use a pore network approach. A pore network model (PNM) is a mesoscale model in which the pore space is represented as a network of pores connected by channels (called throats or bonds). The main advantage of the pore network approach in the context of the present article is that it permits to explicitly represent the porous surface in a discrete way, as in Schlünder's model, whereas also considering crucial additional aspects, such as the spatial variation in pore radius and the coupling with phenomena occurring inside the porous medium.

As described in review papers,[13–15] a pore network model of drying can be more or less sophisticated depending on which phenomena are taken into account. Here, the idea is to consider the simplest situation corresponding to the slow drying at room temperature of a relatively thin sample, a situation frequently encountered in laboratory experiments. Slow drying implies that the temperature variation induced by the evaporation process is negligible. As discussed in Ref. 13, three main regimes can be distinguished depending on the competition between the gravitational, viscous, and capillary forces. The capillary regime considered in this article is a regime in which the phase distribution during drying is essentially controlled by the capillary forces. As discussed in Ref. 6, length scales can be associated with the capillary-gravity regime and the capillary-viscous regime. The capillary regime is the regime observed when both length scales are greater than the height of sample. Thus, this regime is typically observed in samples which are sufficiently thin such that the pressure drop in the liquid phase due to gravity or viscous effects is negligible compared to the pressure variations due to the capillary effects. This is the regime typically observed in many laboratory experiments performed at the room temperature.[2] The capillary regime can be modeled on a network using the algorithm proposed in Ref. 16.

In addition to a better description of the phenomena occurring at the surface, a motivation of the present work is also to better understand the shortcomings of the classical continuum models of drying[17] (for more references see for instance the review chapter[18]). It can be considered that this type of model cannot predict the CRP/FRP transition without introducing some fitting parameters (see the next section). Thus, the question arises as to whether it is intrinsically not possible to do much better than the classical models, or if a better understanding of modeling issues might suggest directions for developing better models.

Finally, the present article can be seen as complementary to the works presented in Refs. 19 and 20. In Ref. 19, we focus on the velocity field induced in the liquid phase during drying, whereas in Ref. 20 we discuss in depth the classical continuum model of drying from comparisons with pore network simulations. In the present article, we thus focus on the phenomena occurring at the surface.

This article is organized as follows: The classical relationship used to express the mass-transfer boundary condition at the surface within the framework of the classical continuum models of drying is recalled in the next section. Then, Schlünder's model is briefly presented. This is followed by recalling the main features of the pore network model. Thereafter, results are presented and discussed, and Schlünder's model is tested against pore network simulations. In the last section, a conclusion is offered.

Coupling of External and Internal Transfer in the Continuum Approach

Before presenting the pore network approach, it is interesting to recall how the coupling between external and internal transport is performed in the classical continuum models of drying, for example, Ref. 17 among others. Classically, the main variable involved in the internal transfer description is the moisture content or equivalently the saturation S ($S=V_l/V_p$, where V_l and V_p are the volume of liquid and volume of the pore space within a representative element, respectively). Considering only situations where the temperature is quasi-uniform and constant (isothermal drying), coupling the external transfer and the internal transfer consists in expressing the continuity of vapor concentration and mass flux at the interface between the porous medium and the external gas. To express the continuity of the vapor concentration (or, equivalently, the vapor partial pressure), a relationship is needed between the saturation at the surface and the vapor concentration in the pore space. This is usually obtained by invoking adsorption phenomena. Thus, the desorption isotherm φ is generally used to provide this relationship

$$\frac{P_v}{P_{vs}} = \phi(S) \tag{1}$$

where P_v and P_{vs} are the vapor partial pressure and saturation vapor pressure, respectively. The vapor flux j at the interface can be expressed as

$$j = -\frac{M_v D}{RT} \nabla P_v \cdot \mathbf{n} \tag{2}$$

where $\mathbf{n}$ is the unit normal vector at the surface. M_v, R, and T are the water molecular weight, the universal gas constant, and the temperature. D is the molecular diffusion coefficient of vapor in the binary mixture formed by air and the vapor. The full coupling approach then requires the solution of the mass transport equation governing the variation of the vapor partial pressure in the external gas.[3] A simpler approach taken in many studies,[17] is to introduce a mass-transfer coefficient h_m and to express Eq. 2 as

$$j = \frac{h_m M_v}{RT} (P_{vi} - P_{v\infty}) \tag{3}$$

where P_{vi} and $P_{v\infty}$ are the vapor pressure at the surface and in the external gas far away from the porous surface, respectively. Expressing the mass-transfer coefficient in terms of external flow parameters, such as the Reynolds or Schmidt numbers, is however generally not sufficient to reproduce the experimental data.[17] The mass-transfer coefficient is actually

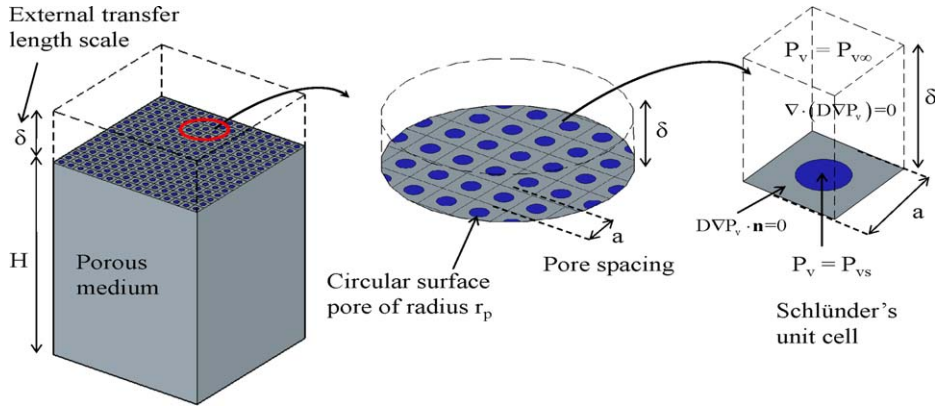

Figure 1. Representation of porous medium surface according to Schlünder's model.[10]

[Color figure can be viewed at wileyonlinelibrary.com]

fitted assuming that it depends on the saturation at the surface. As a result, combining Eqs. 1 and 3 lead to expressing the boundary condition at the interface as

$$j=\frac{h_m(S)M_v}{RT}\left(P_{vs}\phi(S)-P_{v\infty}\right) \tag{4}$$

Actually, Eq. 4 can be considered as one of the weakest points of the current continuum models of drying. Even for simple external flow configurations, similar to a boundary layer flow on a flat plate for instance, there is no theory predicting the functional form of $h_m(S)$. To the best of our knowledge, the most advanced model is actually Schlünder's model. As shown in the next section, this model provides an expression for $h_m(S)$ when it can be considered that mass transfer from the surface is essentially by diffusion through a layer of finite thickness.

Schlünder's Closure Relationship

The porous medium surface considered by Schlünder is illustrated in Figure 1. This is a spatially periodic surface. The unit cell is a parallelepipedic volume in which the mass transfer is governed by diffusion. The bottom surface, which corresponds to the top surface of the porous sample, contains a cylindrical pore entrance where the vapor partial pressure is known (assuming the pore is occupied by liquid, the vapor pressure right above the pore opening is the saturation vapor pressure). A zero flux condition is imposed on the solid surface (surface complementary to pore opening surface). The vapor partial pressure is known at the distance δ from the surface, $P_v=P_{v\infty}$, where δ is the mass boundary layer thickness and $P_{v\infty}$ is the vapor partial pressure in the surrounding air. Spatial periodic boundary conditions are imposed on the lateral sides of the unit cell.

Actually, Schlünder did not solve exactly this problem but a simplified version considering that the liquid formed a half-droplet at the pore entrance. This enabled him to obtain a closed-form solution, which reads

$$\frac{J}{J_{\mathrm{CRP}}}=\frac{1}{1+\frac{2r_p}{\pi\delta}\sqrt{\frac{\pi}{4\theta}}\left[\sqrt{\frac{\pi}{4\theta}}-1\right]} \tag{5}$$

where J is the evaporation rate, J_{CRP} is the evaporation rate when the surface is entirely covered by liquid, r_p is the radius of the openings (pores) at the surface, and $\theta=\frac{\pi r_p^2}{a^2}$ is the wetted fraction of the surface. The model is in principle valid only for $\theta \le \frac{\pi}{4}$ (which corresponds to a circular pore of radius $a/2$). However, using Eq. 5 for greater values of θ, that is, up to $\theta = 1$, does not lead to odd results and thus is permitted from a practical point of view. Hence, Eq. 5 provides an explicit relationship between the evaporation rate and the degree of occupancy of the porous surface by the liquid. A typical variation of J with the surface wetted fraction from Eq. 5 is shown in Figure 2. As typically $\frac{r_p}{\delta} \ll 1$, $J \approx J_{\mathrm{CRP}}$ for θ sufficiently high, whereas $\frac{J}{J_{\mathrm{CRP}}}$ decreases sharply with θ when the surface becomes sufficiently dry. Thus, according to Schlünder's model (noting that $j = J/A$, where A is the area of the porous medium surface)

$$j=\frac{1}{1+\frac{2r_p}{\pi\delta}\sqrt{\frac{\pi}{4\theta}}\left[\sqrt{\frac{\pi}{4\theta}}-1\right]}\frac{\mathrm{M_v}}{RT}\frac{P_{vs}-P_{v\infty}}{\delta} \tag{6}$$

Comparing Eqs. 4 and 6 and assuming that $\theta = S$ at the surface, yields

$$h_m(S)=\frac{1}{1+\frac{2r_p}{\pi\delta}\sqrt{\frac{\pi}{4S}}\left[\sqrt{\frac{\pi}{4S}}-1\right]}\frac{P_{vs}-P_{v\infty}}{P_{vs}\phi(S)-P_{v\infty}}. \tag{7}$$

Equation 7 provides a closure relation giving the variation with saturation of the mass-transfer coefficient at the surface.

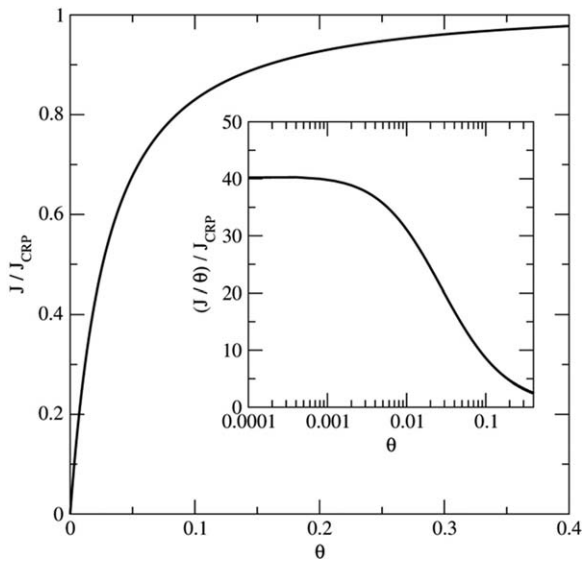

Figure 2. Typical variation of $\frac{J}{J_{\mathrm{CRP}}}$ with surface wetted fraction θ according to the Schlünder's formula ($r_p = 0.5$ mm, $\delta = 10$ mm).

The inset shows the variation of $\frac{J}{\theta J_{\mathrm{CRP}}}$ as a function of θ.

However, determining $h_m(S)$ from Eq. 7 requires knowledge of the desorption isotherm whereas the direct use of Eq. 5 as a closure relationship at the surface does not. Thus, the question arises as to whether the desorption isotherm is a key element in the modeling of the drying process or not.

Another interesting piece of information is the mean evaporation flux from the wetted area of the surface $J/(A\theta)$ (or in dimensionless form $\frac{J}{\theta J_{CRP}}$). $J/(A\theta)$ is proportional to the mean interstitial velocity induced in the liquid within the porous medium, which is a variable of interest when the liquid contains particles, ions, or dissolved species. According to Schlünder's formula

$$\frac{J}{\theta J_{CRP}} = \frac{1}{\theta + \frac{2r_p}{\pi\delta}\sqrt{\frac{\pi\theta}{4}}\left[\sqrt{\frac{\pi}{4\theta}} - 1\right]} \tag{8}$$

The variation of $\frac{J}{\theta J_{CRP}}$ with θ is also shown in Figure 2. As illustrated in Figure 2, and obvious from Eq. 8, $\frac{J}{\theta J_{CRP}} \to \frac{2\delta}{r_p}$ when $\theta \to 0$. Thus, $\frac{J}{\theta J_{CRP}}$ reaches a plateau when θ becomes sufficiently low. The variation of $\frac{J}{\theta J_{CRP}}$ with θ when J varies weakly (i.e., for θ sufficiently large during the quasi-CRP predicted by Eq. 5) illustrates a compensation mechanism: the evaporation rate from the wetted area must increase when θ decreases for the evaporation rate from the porous surface to remain approximately constant (CRP). According to Schlünder's model, the increase in the evaporation flux from the wetted area compensates the decrease in the mass-transfer rate from pores becoming dry at the surface, so that the total evaporation rate is not affected during the CRP.

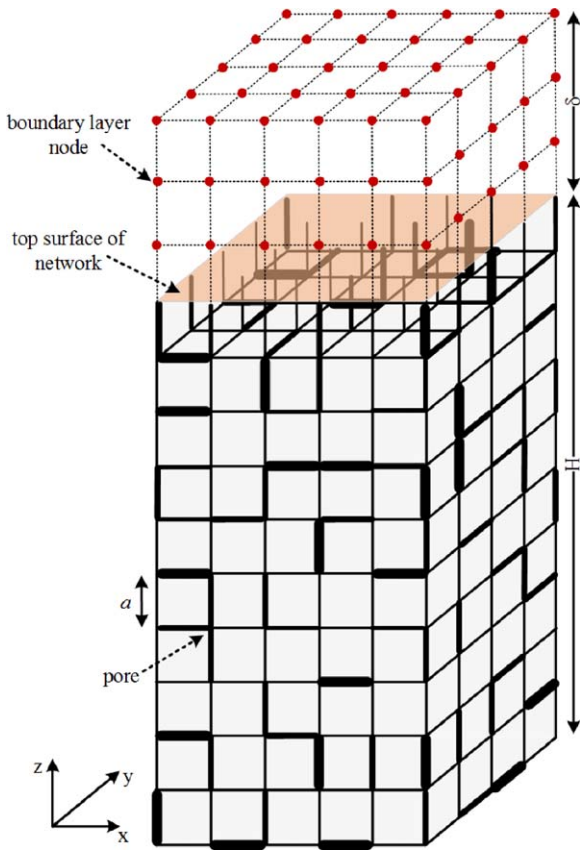

Figure 3. Sketch of a cubic pore network with external mass-transfer layer on top.

[Color figure can be viewed at wileyonlinelibrary.com]

Table 1. Parameters for PN Drying Simulations

Parameter	Value
Pore network size	25 × 25×51 nodes
Boundary layer	25 × 25×10 nodes
Number of realizations	15
Mean throat radius	250 μm
Standard deviation of throat radius	25 μm
Throat length (lattice spacing)	1 mm
Temperature	20°C
Gas pressure	1 atm
Porosity	0.594
Top surface porosity ε_s	0.2
Gas saturation at BT	0.097

The value of top surface porosity ε_s is obtained by dividing the summation of cross-sectional area of top vertical throats $\sum_{i=1}^{N_x N_y} \pi r_i^2$ by the cross-section area of the network ($N_x N_y a^2$) and is (about) 1/3 of the porosity of the network.

Pore Network Model of Drying (Capillary Regime)

Pore network structure

As considered in several previous studies,[18,21] and depicted in Figure 3, we use a cubic network of volumeless pores interconnected by cylindrical channels (throats). The evaporative surface is on top. The bottom surface is sealed. Periodic boundary conditions are imposed on the lateral faces of the network. The distance between two pores, referred to as the lattice spacing a, is constant whereas the radii r_t of cylindrical throats are randomly distributed according to a Gaussian distribution. The values of the main network parameters used here are summarized in Table 1. It can be argued that that throat size distributions (TSDs) are often not Gaussian in natural or manufactured porous media. However, we believe that the main results of the paper are generic, that is, not significantly dependent on the exact form of the TSD. Nevertheless, it would be interesting to study the impact of the TSD type on the results in future works.

As indicated in Table 1, we use a network of 25 × 25×51 nodes, with 51 nodes in the vertical direction. The diffusive external boundary is represented by adding 25 × 25×10 nodes on top of this network. The discretization step in the boundary layer is equal to the lattice spacing a. The boundary layer is shown in Figure 3. For this series of simulations, 15 different realizations of the same throat size Gaussian probability density function are considered.

Drying algorithm

The drying process is characterized by the formation of liquid clusters (at the very beginning there is only one liquid cluster, the network being assumed fully saturated when drying starts). The drying algorithm for simulating the capillary regime[16] takes into account the formation of clusters and is based on the combination of the invasion percolation algorithm,[22] applied to each cluster, and the computation of the evaporation rate of each cluster. The latter is obtained from a finite-volume like solution of the vapor diffusion problem on the network (and in the external boundary layer on top of the network). One can refer to Ref. 23 for more details of the vapor diffusion computation. This drying algorithm can be summarized as follows:

1. every liquid cluster present in the network is identified;
2. the interfacial throat of lowest capillary threshold is identified for each cluster, the volume of liquid contained at time t in this element is V_{sc};

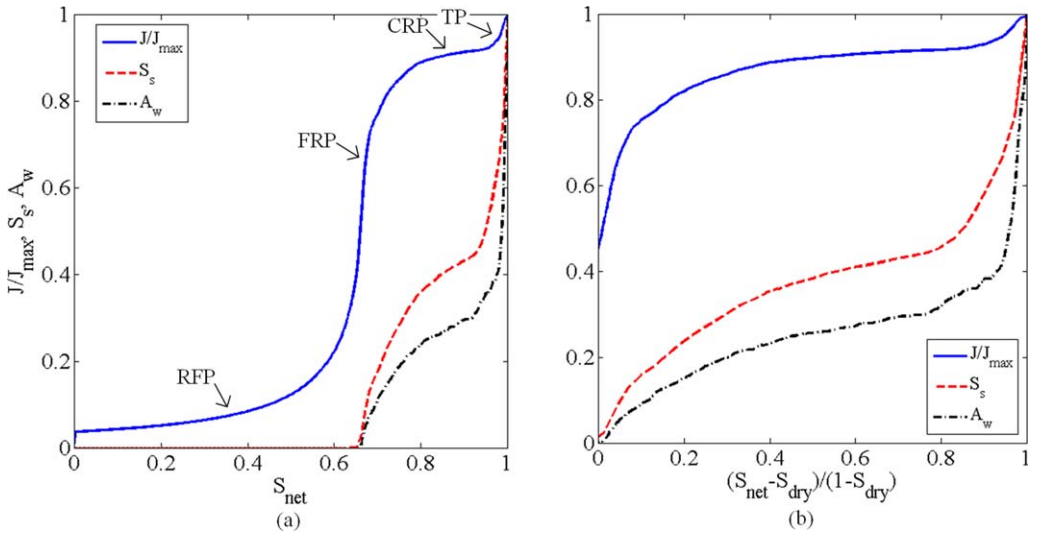

Figure 4. Normalized evaporation rate, surface pore occupancy ratio A_w, and surface saturation S_s averaged over 15 realizations as functions of (a) network overall saturation and (b) reduced network saturation calculated as $(S_{net} - S_{dry})/(1 - S_{dry})$ with $S_{dry} = 0.656$.

[Color figure can be viewed at wileyonlinelibrary.com]

3. the evaporation flux F_c at the boundary of each cluster is obtained from the finite-volume like computation of liquid vapor partial pressure in the gas phase;
4. for each cluster, the time t_c required to evaporate the amount of liquid contained in the throat identified in step (2) is computed by $t_c = \frac{\rho_\ell V_{sc}}{F_c}$;
5. the throat among the throats selected in step (2) eventually invaded is that corresponding to $t_{c\min} = \min(t_c)$;
6. the phase distribution within the network is updated, which includes the partial evaporation of liquid contained in the throats selected in step (2) with $\rho_\ell V_\ell(t + t_{c\min}) = \rho_\ell V_\ell(t) - F_c t_{c\min}$ (where ρ_ℓ is the liquid density and V_ℓ the volume of liquid contained in the element) except for the throat selected in step (5) which becomes completely saturated by the gas phase.

The procedure can be repeated until complete drying of the network or it can be stopped at some intermediate stage. The capillary threshold mentioned in step (2) is the throat capillary entry pressure, which is expressed as (assuming perfect wetting between liquid and solid)

$$p_{cth} = \frac{2\gamma}{r_t} \tag{9}$$

where γ is the surface tension. The coupling between the network and the external boundary layer is straightforward as the vapor diffusion problems in the network and in the boundary layer are solved together by numerical solution of a single linear system containing both the network nodes and the boundary layer nodes, see again Ref. 23 for more details.

Simulation Results

Drying kinetics

The normalized evaporation rate curve obtained from the simulation averaged over the 15 realizations of the TSD is shown in Figure 4. The classical three main periods can be identified. One can note, however, the existence of an additional initial short period in which the evaporation rate drops. In this short period, referred to as the initial transition period (TP) in Ref. 24, the gas phase has not yet reached the bottom of the network. This period is sometimes attributed to the evaporation of a liquid film at the surface. Our simulation although indicates that this period can also be observed with no liquid film present when drying starts. The breakthrough (BT) situation, when the gas phase reaches the network bottom for the first time, occurs for $S_{BT} = 0.903$. The saturation at BT is expected to be very close to 1 in real systems, which explains why this initial period is often not seen in experiments. As discussed in more details in Ref. 19, the fact that this period is visible here is a consequence of the relatively small network considered. As can also be seen, the evaporation rate is actually not perfectly constant during the "CRP," which starts when the saturation is about 0.97, that is, before BT.

The decrease in the evaporation rate after the CRP can be related to the presence of liquid at the surface. The latter is characterized by the surface pore occupancy ratio A_w defined as

$$A_w = \frac{\sum_{i=1}^{n} \pi r_i^2}{\sum_{i=1}^{N_x N_y} \pi r_i^2} \tag{10}$$

where n is the number of vertical channels (throats) occupied by liquid at the top surface of the network and $N_x N_y$ is the total number of vertical channels at the network top surface. Thus, A_w changes from one (fully wet surface, meaning that all surface throats are occupied by liquid) to zero (fully dry surface). As can be seen, A_w decreases sharply during the initial TP of drying down to about $A_w = 0.4$ (i.e., before the onset of the CRP). Thus, approximately 60% of the vertical channels at the surface are invaded by the gas phase during this period. Then, the decrease of A_w with S_{net} is much slower (this corresponds to the CRP). The variation rate of A_w with S_{net} increases again during the FRP. All the vertical channels are invaded at the network top surface when S_{net} is around 0.656. This value, denoted by S_{dry} ($S_{dry} = 0.656$), is high and related to the

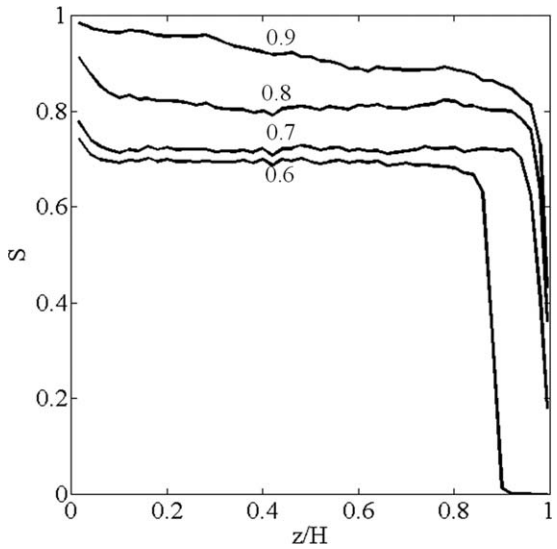

Figure 5. Saturation profiles of capillary-dominated drying obtained from PN simulations and averaged over 15 realizations.

From the top, profiles corresponding to network saturations of 0.9, 0.8, 0.7, and 0.6, respectively. The network top surface is on the right ($z/H = 1$).

irreducible saturation (saturation when the liquid phase does not percolate anymore from top to bottom), which is quite high in a cubic network compared to real systems characterized by higher coordinance (the coordinance, i.e., the number of first neighbor pores to a given pore, is six in a simple cubic network). Also, the irreducible saturation is high here because all the liquid is in throats in the used PNM (pores are volumeless). As can be seen from Figure 4b, showing the normalized evaporation rate as a function of reduced saturation $(S_{net} - S_{dry})/(1 - S_{dry})$, the CRP approximately corresponds to A_w in the range [0.2–0.4]. We have also plotted in Figure 4 the variation of surface saturation S_s, which is computed by summing up the liquid volume in all of the top horizontal and vertical throats plus half of the second top vertical throats and dividing it by the total pore space volume in this slice. As expected, its variation is quite similar to the one observed for A_w.

Saturation profiles: Edge effects

As discussed in Ref. 19, the capillary regime is characterized by spatially quasi-uniform saturation profiles during the CRP over almost all the height of network. This is illustrated in Figure 5 with horizontal slice-averaged saturation. Each slice contains one horizontal plane of pores and horizontal throats and half of the volume of the vertical throats (above and below) connected to the considered plane of pores (except the very first slice which, as mentioned before, contains not half but the full volume of vertical throats connected to the network surface).

As can be seen from Figure 5, the saturation profiles during the CRP are characterized by edge effects on both the evaporative top side and the sealed bottom side. The edge effect of main interest for the present article is on the side of the evaporative surface (on the right in Figure 5). As discussed in Ref. 19, this edge effect seems not to be due to the small size of our network but an intrinsic feature of the drying process as qualitatively similar edge effects are also seen in the saturation profiles measured by NMR in real samples, that is, Refs. 25 and [26]. The size of the edge effect (right side) is in the order of 4–5 lattice spacing units in the case of our network. However, the spatial extent of edge effect might depend on the network size and this possible finite size effect would be worth analyzing. This edge effect is not captured by the traditional continuum model of the drying process,[27] which predicts a spatially uniform saturation all along the sample height in the capillary regime. The variation of surface saturation S_s with S_{net} is depicted in Figure 4.

The top edge effect actually begins to form in the initial TP. Thus both phenomena, that is, the TP and the top edge effect, are actually interrelated. It is because of the preferential invasion of the upper layer of the medium by the gas phase that the evaporation rate decreases during the initial TP. As illustrated in Figure 4, the variation of the saturation in the first layer (S_s), is significantly more pronounced in the TP compared to the CRP (which is thus explained in part by the fact that the change in pore occupancy in the upper layer of the medium becomes much more slower with decreasing network saturation).

Surface clustering

Phase distributions at the surface of the network for the capillary-dominated regime for various values of A_w are shown in Figure 6. As discussed in previous papers,[28] the drying process is characterized by the formation of liquid clusters, whose residence time in the network depends on the position of the cluster within the network and its size. The deeper in the network the cluster is, the longer its presence in the network. As a result, liquid throats at the surface can belong to different clusters. This is illustrated in Figure 6 where the different colors correspond to liquid surface throats belonging to various liquid clusters, whereas white color indicates gas pores. Note that the different colors correspond to "surface" liquid clusters, also referred to as wet patches. A surface cluster is defined as a set of throat openings at the surface which are first neighbors and surrounded by gas throats. Two surface clusters can actually belong to the same network liquid cluster, also referred to as an "in-volume" cluster, if they are interconnected deeper in the network. In what follows, only surface clusters are considered without consideration of their possible in depth interconnection. However, this feature will be further illustrated in Figure 11 below.

As shown in Ref. 28, the number of in-volume clusters increases all along the CRP until the main (i.e., biggest) cluster ceases to be connected to the network top surface. This progressive splitting of the liquid phase into various clusters is also illustrated in Figure 7 showing the variation of the total number of wet patches at the surface as a function of the surface pore occupancy ratio. As can be seen from Figure 7 in conjunction with Figure 4, the number of surface clusters significantly increases during the CRP. Then, this number approximately stabilizes (short plateau on the left of the maximum in Figure 7) around the CRP/FRP transition ($A_w \cong 0.2$) before dropping sharply during the FRP. The mean surface area $\bar{A}_{wp}$ and the standard deviation of surface area of wet patches normalized by the total surface pore (throat) area $A_t = \sum_{i=1}^{N_x N_y} \pi r_i^2$ are shown in Figures 8 and 9. At the beginning of the drying process, there is only one wet patch. As soon as the second wet patch has been produced, the standard deviation $_{wp}$ becomes nonzero and the decrease in $\bar{A}_{wp}$ deviates from linearity. As the drying process goes on, wet patches with different sizes are created which leads to a maximum in the $_{wp}$ curve.

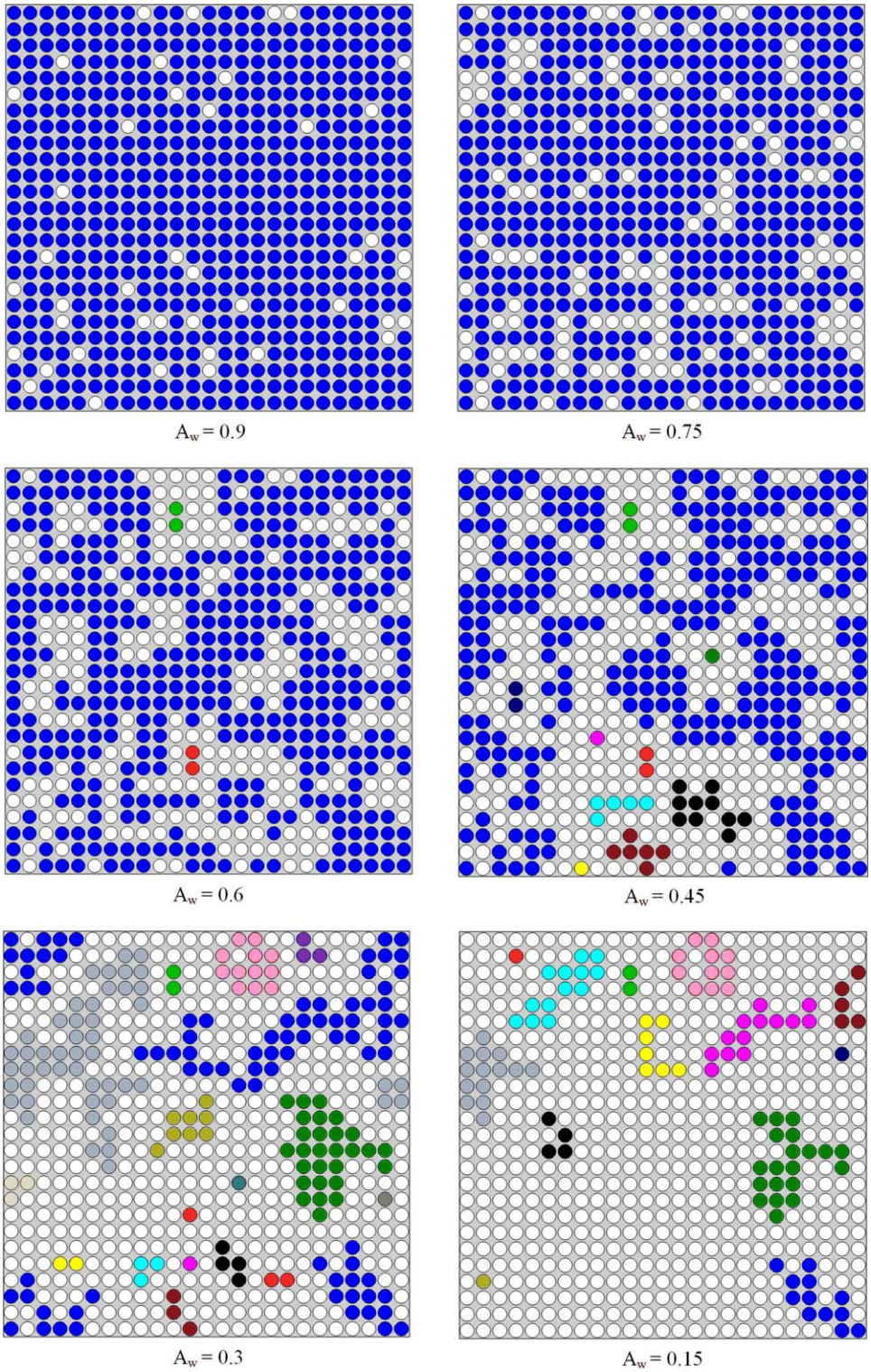

Figure 6. Phase distribution at the surface for various values of A_w.

White color indicates gas pores, while the other colors show the liquid in different surface liquid clusters. The results were obtained from one realization. [Color figure can be viewed at wileyonlinelibrary.com]

After this point, with consecutive drying of all wet patches, their surface area and its normalized standard deviation constantly decrease. At low surface pore occupancy ratio, the wet patches have more uniform and smaller size. Again, it is interesting to see that most of the variations depicted in Figures 8 and 9 correspond to the very first period before the CRP onset.

The wet patches size distribution is illustrated in Figure 10 (histogram over 15 realizations) and Figure 11 (for the realization corresponding to Figure 6) when the standard deviation $_{wp}$ reaches its maximum. As can be seen, the corresponding cluster distribution at the surface is essentially characterized by one big cluster (in blue in Figure 11a) and several much

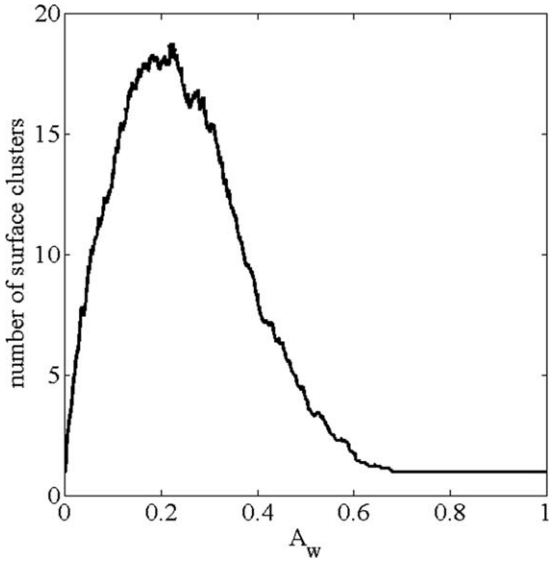

Figure 7. Variation of the total number of wet patches at the surface as a function of surface pore occupancy ratio A_w averaged over 15 realizations.

smaller clusters. Figure 11 also illustrates the fact that different surface clusters (wet patches) can actually belong to the same in-volume cluster. As can be seen, there are three in-volume clusters connected to the surface (corresponding to the throat openings shown in blue, green, and black in Figure 11b) while the number of wet patches is seven (Figure 11a).

Contrary to the simplified surface illustrated in Figure 1, three phases, namely liquid, gas, and solid coexist at the surface of a drying porous medium during the CRP and the FRP, and not simply two. It is therefore interesting to characterize the relative contribution of each corresponding surface area to the total mass flow rate. The contribution of solid surface is obviously zero. The evaporation rate can thus be actually decomposed into two components

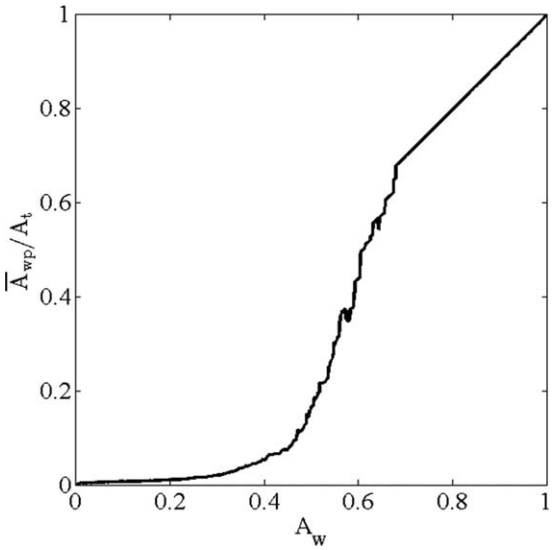

Figure 8. The normalized mean surface area of wet patches vs. surface pore occupancy ratio A_w averaged over 15 realizations.

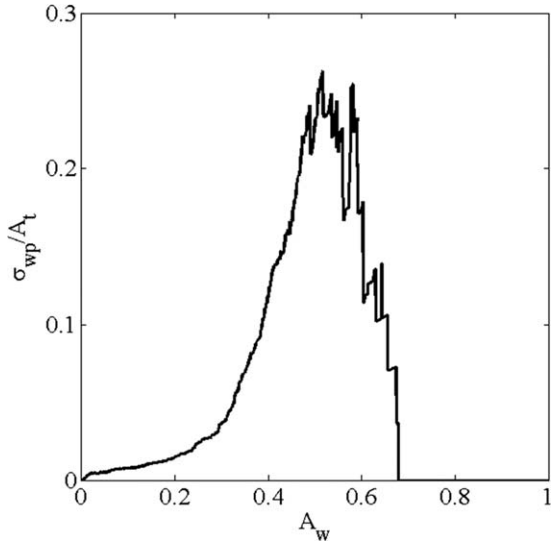

Figure 9. The normalized standard deviation of surface area of wet patches vs. surface pore occupancy ratio A_w averaged over 15 realizations.

$$J = J_{\text{wet}} + J_{\text{dry}}, \tag{11}$$

where J_{wet} is the evaporation rate from the wet areas at the surface and J_{dry} is the mass-transfer rate from the openings of dry throats at the surface. Thus, J_{dry} corresponds to internal evaporation, that is, from the surface of menisci which have receded into the network. The relative contributions of the wet and dry patches to the total drying rate are shown in Figure 12. The transition between the dominant contributing areas to the total mass-transfer rate at the surface happens at surface pore occupancy ratio equal to roughly 0.3, thus during the CRP (see Figure 4). Evaporation rate is bigger in the wet region, as vapor

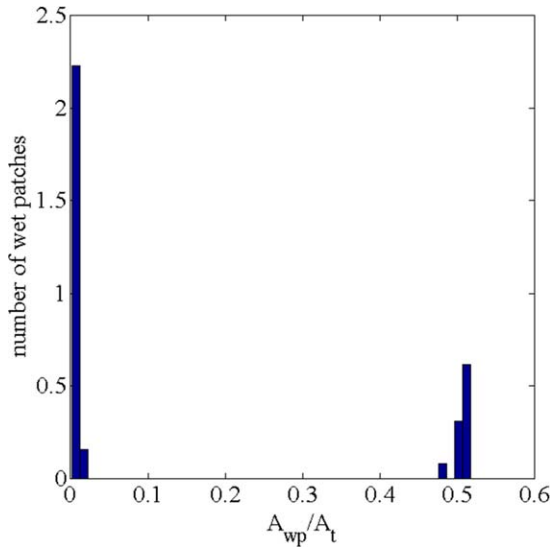

Figure 10. Histogram of normalized wet patches size (A_{wp}/A_t) distribution when the standard deviation of wet patches size $_{wp}$ is at its maximum.

The histogram has been averaged among all realizations. The maximum in $_{wp}$ occurs at $A_w = 0.52$ (Figure 9). [Color figure can be viewed at wileyonlinelibrary.com]

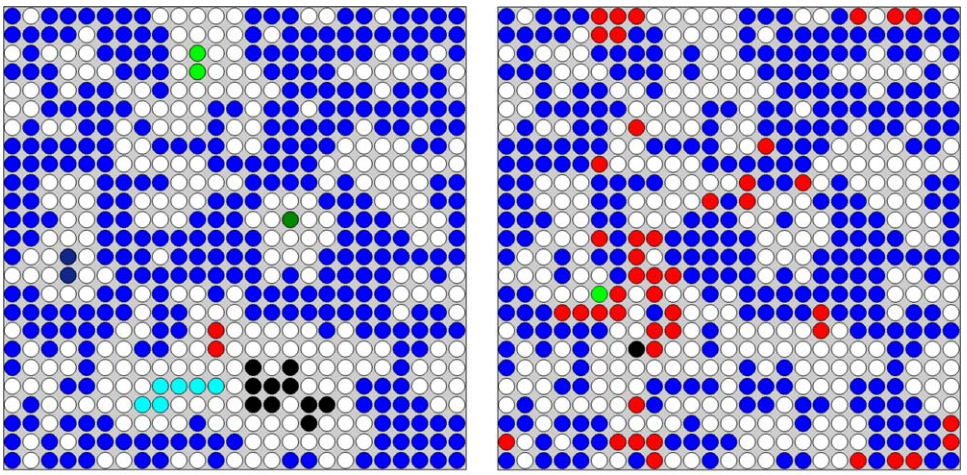

Figure 11. Phase distribution at the surface when the standard deviation of wet patch sizes is at its maximum.

White color indicates a vapor pore, whereas in (a) each surface cluster is shown with a different color and in (b) each in-volume cluster is shown with a different color, while menisci belonging to isolated top vertical throats are in red. For producing this figure, the same realization as in Figure 6 was considered. [Color figure can be viewed at wileyonlinelibrary.com]

pressure at the pore entrances in this region is the saturation vapor pressure. Therefore, the dry region needs a bigger area to equalize the evaporation rate from the wet area. This is why the transition happens at A_w smaller than 0.5.

Based on Figures 4 and 12, it is interesting to observe that the CRP in this example corresponds to a regime in which the most important contribution to mass transfer is initially from the liquid pores at the surface ($A_w \cong 0.4$) and progressively comes from the dry pores as the CRP/FRP transition ($A_w \cong 0.2$) is approached.

Compared to Schlünder's analysis,[10] a major difference is therefore that the dry pores greatly contribute to the mass transfer in the CRP and the FRP. A similar observation is reported in Ref. 29 where PNM simulations are compared to the even more simplified model proposed in Ref. 9.

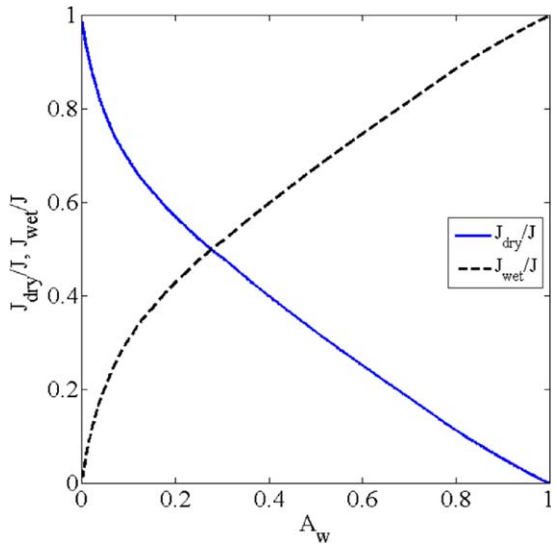

Figure 12. Relative contributions of dry and wet regions at the surface to the total mass-transfer rate vs. surface pore occupancy ratio A_w averaged over 15 realizations.

[Color figure can be viewed at wileyonlinelibrary.com]

Vapor partial pressure at the surface

The average vapor partial pressure at the surface is computed as

$$P_v^* = \frac{\sum_{i=1}^{N_x N_y} \pi r_i^2 P_{vi}}{\sum_{i=1}^{N_x N_y} \pi r_i^2} \tag{12}$$

weighted by the surface of the throat cross-section surface area at the top surface of the network. As can be seen from Figure 13, P_v^* is lower than the saturation vapor pressure P_{vs} over most of the FRP and CRP, that is, in the presence of liquid water at the surface. Hence, P_v^* varies as a function of A_w.

In the initial TP of drying, isolated throats form at the top of the network and are dried out one by one. Thus, the pores at the surface which are connected to those throats will not be in contact with liquid water and therefore their vapor pressures become smaller than the saturation vapor pressure. As the drying goes on, more and more pores are out of equilibrium with the liquid, which will consequently affect the total evaporation rate of the sample.

As discussed earlier, the fact that the spatially averaged vapor pressure is different from the saturation vapor pressure in the presence of liquid water is traditionally explained in the continuum approach to drying,[17,27] by adsorption and capillary condensation phenomena and modeled by invoking the Kelvin effect. The Kelvin effect refers to the modification of the equilibrium vapor pressure at the surface of a curved meniscus.[30] The Kelvin's effect is typically significant only in very small pores (on the order of a few tens of nanometers or less). These phenomena are not taken into account in our pore network model, because in capillary porous media the pore sizes are in the micrometric range, thus much greater. Therefore, as discussed in Ref. 20 in detail, the curve depicted in Figure 13a cannot be interpreted as a desorption isotherm. The fact that

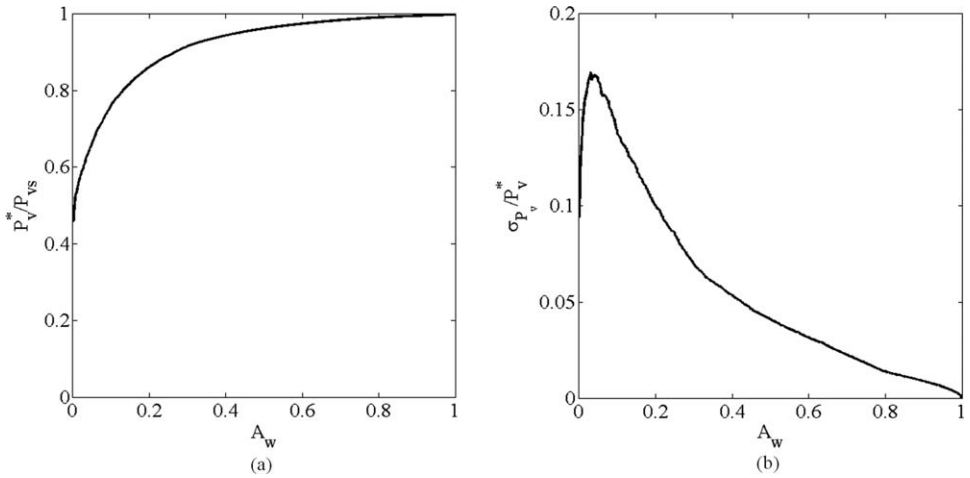

Figure 13. (a) Variation of P_v^* (Eq. 12) as a function of surface pore occupancy ratio A_w; P_{vs} is the saturation vapor pressure and (b) normalized standard deviation of vapor pressure at the surface vs. surface pore occupancy ratio A_w.

These results are averages over 15 realizations.

P_v^* is lower that P_{vs} in Figure 13a is interpreted as the signature of a nonlocal equilibrium effect. Although considered by some authors,[31,32] nonlocal equilibrium effects are not taken into account in the traditional models of drying of capillary porous media.[17,27] On the contrary, traditional models are based on the local equilibrium assumption, that is, the average vapor pressure in a representative elementary volume (or at the surface) is the same as at the surface of menisci.

Figure 13b shows the standard deviation of the vapor pressure at the surface vs. the surface pore occupancy ratio A_w. The standard deviation of the vapor pressure increases constantly until it reaches a maximum. At this point, a small part of the surface is wet, while the rest is dry and pores have different vapor pressures. After this point, the wet area dries out which makes the vapor pressure of surface pores more uniform. As can be seen from Figures 4 and 13, the CRP actually occurs ($A_w \cong 0.4$) when the average vapor pressure at the surface starts decreasing sharply. The maximum in vapor pressure variability at the surface (which corresponds to the standard deviation maximum in Figure 13b) approximately corresponds to the end of the FRP.

Test of Schlünder's Model

To use Schlünder's formula (Eq. 5), we need to define the three parameters θ, δ, and r_p. There is no problem regarding δ, which is given in Table 1 ($\delta = 10a$). More difficult is the definition of θ and r_p, owing to the assumptions made in the pore network modeling for the computations of the external mass transfer.

As sketched in Figure 14, the external mass transfer is actually computed assuming that all the surface of each unit cell containing a liquid throat is at saturation vapor pressure and not only the throat opening surface area.

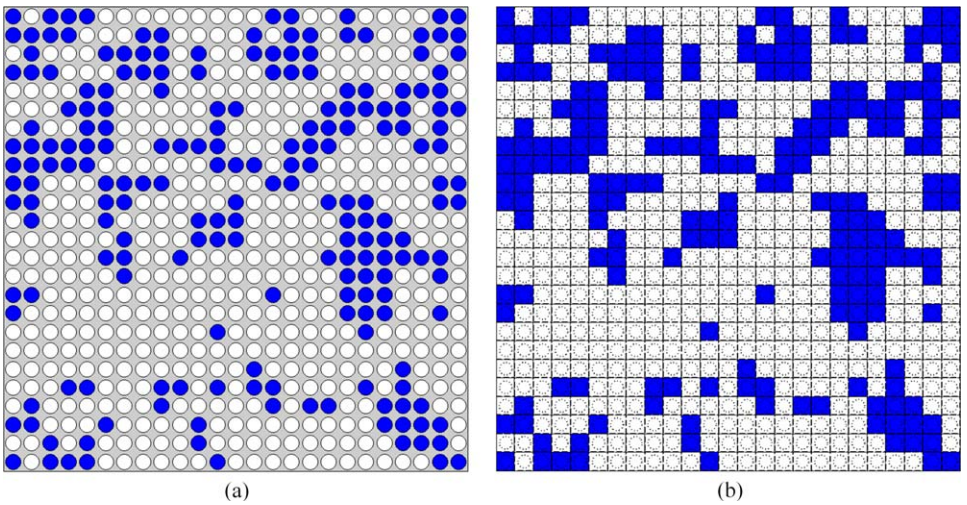

Figure 14. (a) Sketch of the pore network surface with liquid throat openings in blue and (b) the surface actually considered for the computation of the external mass transfer (the saturation vapor pressure is imposed all over the surface in blue and not only over the liquid throat opening surface).

[Color figure can be viewed at wileyonlinelibrary.com]

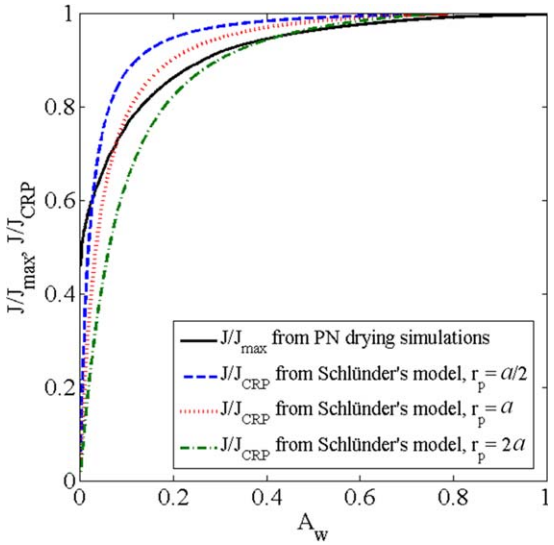

Figure 15. The normalized evaporation rate obtained from PN drying simulations averaged over 15 realizations and the normalized evaporation rate predicted by Eq. 5 vs. surface pore occupancy ratio A_w for different r_p; θ is calculated from Eq. 13.

[Color figure can be viewed at wileyonlinelibrary.com]

As a result, θ is defined as

$$\theta = \frac{n}{N_x N_y} \tag{13}$$

where n is the number of wet pores at the surface, while r_p is set equal to $a/2$, which corresponds to the radius of the circle that fits into a square of side length a (see Figure 1).

As can be seen in Figure 15, using Schlünder's model for these parameter values does not lead to good agreement with the PNM results. It can be argued that the average size of the wet patches is actually greater than a because the liquid surface clusters forming at the surface typically contain more than one pore opening (as illustrated in Figures 6 and 14). However, Figure 15 shows that increasing r_p is not sufficient to obtain a good representation of the PNM results with Schlünder's formula.

Figure 16 shows the variation of the mean evaporation rate when it is (incorrectly) assumed that all the mass transfer takes place from the wetted area at the surface. Contrary to Schlünder's model, one can observe a strong change in J/θ as the surface becomes dry. This is so because the major contribution to mass-transfer rate at the surface is actually from the dry pores and not from the wet pores when A_w is sufficiently low (as illustrated in Figure 12). It can be seen, however, that Schlünder's model describes reasonably well the compensation mechanism during the CRP (which corresponds to A_w in the range of [0.2–0.4]).

This is further illustrated in Figure 17 showing the variations of the mean mass-transfer rate at the surface from the dry pores and the wet pores separately. As can be seen, and contrary to Schlünder's model, the mean evaporation rate from the wetted area (J_{wet}/θ) does not reach a plateau for sufficiently low A_w. It continuously increases as the wetted area decreases at the surface. As the average velocity induced in the liquid phase connected to the surface is directly proportional to J_{wet}/θ, this indicates a result markedly different from Schlünder's approach, namely a significant increase in this velocity rather than a stabilization. By contrast, the mean mass-transfer rate from the dry pores slowly decreases all along the CRP and FRP, reflecting the decrease in vapor partial pressure depicted in Figure 13.

Summary and Conclusions

The pore network simulations of drying presented in this study shed light on the phenomena taking place at the surface of a non-hygroscopic porous medium during drying. The drying process is characterized by the formation of wet and dry patches at the porous surface. The number of wet and dry patches at the surface and their statistical properties vary during the drying process. Both types of patches actually contribute to the mass transfer from the surface. This is a significant difference with Schlünder's approach, which essentially hypothesizes that the contribution of dry pores to mass transfer is negligible compared to the evaporation from the wetted area through the so-called compensation mechanism. Also, it can be noted that Schlünder's model assumes a simple spatially periodic structure, which seems to be a too rough approximation in view of the random distribution of clusters of various size at the surface. As a result, the simple parameterization of the evaporation rate as a function of the degree of occupancy of the surface by the liquid proposed by Schlünder does not lead to satisfactory results. More refined modeling approaches are needed to couple properly the internal mass transfer, that is, within the porous medium, and the external mass transfer, for example, in the external boundary layer.

In the example considered, the transition from a dominant contribution to the evaporation rate from the surface wet area to a dominant contribution from the surface dry area occurs during the CRP. The simulations indicate a noticeable edge effect. The saturation increases with the distance from the surface in a thin layer adjacent to the surface until it reaches the bulk saturation (which is spatially uniform in the drying

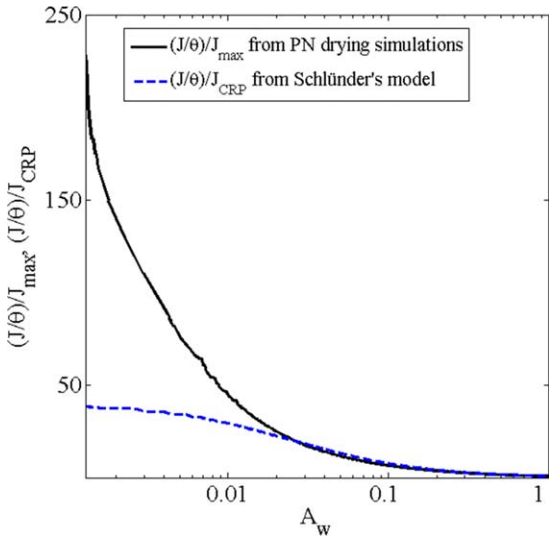

Figure 16. The normalized evaporation rate obtained from PN drying simulations averaged over 15 realizations divided by θ and the normalized evaporation rate predicted by Eq. 8 divided by θ vs. the surface pore occupancy ratio; θ is calculated from Eq. 13.

[Color figure can be viewed at wileyonlinelibrary.com]

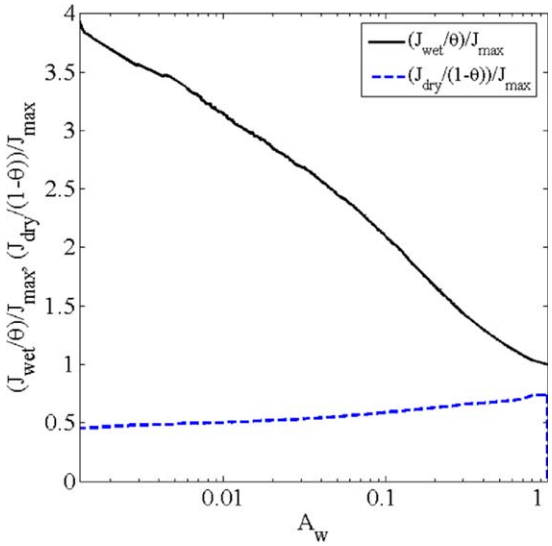

Figure 17. The normalized evaporation rates of the wet and dry regions at the surface obtained from PN drying simulations divided by θ and $(1 - \theta)$, respectively, vs. the surface pore occupancy ratio; θ is calculated from Eq. 13 and the results are averaged over 15 realizations.

[Color figure can be viewed at wileyonlinelibrary.com]

regime considered in this article). The edge effect occurs during the initial TP and it actually explains the drop in the evaporation rate observed in this very short initial period. The edge effect should also be taken into account in the development of models coupling the internal and the external transfer. This probably implies the need to consider the interface between the porous medium and the external air not simply as a surface but as an interfacial layer of finite thickness.

The average vapor partial pressure above the partially wet surface is not the saturation vapor pressure owing to the lower vapor partial pressure in the dry pores at the surface. This has nothing to do with adsorption phenomena, that is, the Kelvin effect. The discrepancy between the average vapor partial pressure and the saturation pressure is, instead, interpreted as a nonlocal equilibrium effect. This is in contrast with the classical continuum models of drying, which are actually based on the local equilibrium assumption. It strongly suggests the need to develop nonlocal equilibrium (or two equation) versions of the continuum model for better and more consistent predictions of the drying process in non-hygroscopic materials.

The main outcome of this article is therefore to propose directions for future research. In brief, better continuum models of the drying process can be expected from the adequate consideration of the nonlocal equilibrium effect, and the edge effect, and from the development of better closure relationships between the mass-transfer rate at the surface and the degree of occupancy of the porous surface by the liquid than provided by Schlünder's model.

This study is implicitly based on the assumption that the impact of corner liquid films,[33,34] is negligible as the presence of such films is not taken into account in the pore network model considered in this article. The case with a significant impact of secondary capillary liquid structures, such as corner liquid films, would deserve a specific study along the same lines as the present one.

Although we believe that the bottlenecks identified in the study are generic, it would be interesting to develop still more refined simulations in order to obtain more accurate results. For example, the mesh used to discretize the external mass-transfer problem is coarse as its discretization step is the same as the lattice spacing. This can be questioned. It would be desirable to use more refined meshes for the external mass-transfer computation. Also, the impact of several parameters, such as network size or mass boundary layer thickness, would deserve to be studied in future work.

Acknowledgment

This work was financed by the German Research Foundation [Deutsche Forschungsgemeinschaft (DFG)] within the Graduate School 1554 "Micro-Macro-Interactions in Structured Media and Particulate Systems."

Literature Cited

1. Lewis WK. The rate of drying of solid materials. *Ind Eng Chem.* 1921;13(5):427–432.
2. Ceaglskeand NH, Hougen OA. Drying granular solids. *Ind Eng Chem*. 1937;29:805–813.
3. Defraeye T. Advanced computational modelling for drying processes - a review. *Appl Energy*. 2014;131:323–344.
4. Van Brakel J. Mass transfer in convective drying. In: Mujumdar AS, editor. *Advances in Drying*. New York: Hemisphere, 1980:217–267.
5. Coussot P. Scaling approach of the convective drying of a porous medium. *Eur Phys J B*. 2000;15(3):557–566.
6. Lehmann P, Assouline S, Or D. Characteristic lengths affecting evaporative drying of porous media. *Phys Rev E*. 2008;77(5, Pt 2): 056309.
7. Shokri N, Or D. What determines drying rates at the onset of diffusion controlled stage-2 evaporation from porous media? *Water Resour Res.* 2011;47(9):W09513.
8. Krischer O, Kröll K. *Die wissenschaftlichen grundlagen der trocknungstechnik*. Berlin: Springer-Verlag, 2013.
9. Suzuki M, Maeda S. On the mechanism of drying of granular beds. *J Chem Eng Jpn*. 1986;1:26–31.
10. Schlünder EU. On the mechanism of the constant drying rate period and its relevance to diffusion controlled catalytic gas phase reactions. *Chem Eng Sci*. 1988;43(10):2685–2688.
11. Haghighi E, Shahraeeni E, Lehmann P, Or D. Evaporation rates across a convective air boundary layer are dominated by diffusion. *Water Resour Res.* 2013;49:1602–1610.
12. Lehmann P, Or D. Effect of wetness patchiness on evaporation dynamics from drying porous surfaces. *Water Resour Res*. 2013;49: 8250–8262.
13. Prat M. Recent advances in pore-scale models for drying of porous media. *Chem Eng J*. 2002;86(1–2):153–164.
14. Metzger T, Tsotsas E, Prat M. Pore network models: a powerful tool to study drying at the pore level and understand the influence of structure on drying kinetics. In: Mujumdar AS, Tsotsas E, editors. *Modern Drying Technology, Computational Tools at Different Scales, Vol*. 1. Hoboken, NJ: Wiley, 2007.
15. Prat M. Pore network models of drying, contact angle, and film flows. *Chem Eng Technol*. 2011;34:1029–1038.
16. Prat M. Percolation model of drying under isothermal conditions in porous media. *Int J Multiphase Flow*. 1993;19(4):691–704.
17. Chen P, Pei DCT. A mathematical model of drying processes. *Int J Heat Mass Transfer*. 1989;32:297–310.
18. Geoffroy S, Prat M. A review of drying theory and modelling approaches. In: Delgado JMPQ, editor. *Drying and Wetting of Building Materials and Components, Building Pathology and Rehabilitation, Vol*. 4. Berlin: Springer, 2014.
19. Moghaddam AA, Kharaghani A, Tsotsas E, Prat M. Kinematics in a slowly drying porous medium: reconciliation of pore network simulations and continuum modeling. *Phys Fluids*. 2017;29:022102.
20. Moghaddam AA, Prat M, Tsotsas E, Kharaghani A. Evaporation in capillary porous media at the perfect piston-like invasion limit: evidence of non-local equilibrium effects. *Water Resour Res*., submitted for publication.

21. Metzger T, Irawan A, Tsotsas E. Influence of pore structure on drying kinetics: a pore network study. *AIChE J*. 2007;53(12):3029–3041.
22. Wilkinson D, Willemsen JF. Invasion percolation: a new form of percolation theory. *J Phys A: Math Gen*. 1983;16:3365–3376.
23. Metzger T, Irawan A, Tsotsas E. Isothermal drying of pore networks: influence of friction for different pore structures. *Dry Technol*. 2007;25(1):49–57.
24. Defraeye T, Blocken B, Derome D, Nicolai B, Carmeliet J. Convective heat and mass transfer modelling at air–porous material interfaces: overview of existing methods and relevance. *Chem Eng Sci*. 2012;74:49–58.
25. Faure P, Coussot P. Drying of a model soil. *Phys Rev E*. 2010;82(3, Pt 2):036303.
26. Gupta S, Huinink H, Prat M, Pel L, Kopinga K. Paradoxical drying due to salt crystallization. *Chem Eng Sci*. 2014;109:204–211.
27. Whitaker S. Simultaneous heat, mass, and momentum transfer in porous media: a theory of drying. *Adv Heat Transfer*. 1977;13:119–203.
28. Bray YL, Prat M. Three dimensional pore network simulation of drying in capillary porous media. *Int J Heat Mass Transfer*. 1999; 42:4207–4224.
29. Yiotis AG, Tsimpanogiannis IN, Stubos AK, Yortsos YC. Coupling between external and internal mass transfer during drying of a porous medium. *Water Resour Res*. 2007;43(6):W06403.
30. Adamson AW. *Physical Chemistry of Surfaces*, 6th ed. Hoboken, NJ: Wiley, 1997.
31. Benet JC, Jouanna P. Non equilibre thermodynamique dans les milieux poreux non satures avec changement de phase. *Int J Heat Mass Transfer*. 1983;26:1585–1595.
32. Pujol A, Debenest G, Pommier S, Quintard M, Chenu D. Modeling composting processes with local equilibrium and local non-equilibrium approaches for water exchange terms. *Dry Technol*. 2011;29(16):1941–1953.
33. Chauvet F, Duru P, Geoffroy S, Prat M. Three periods of drying of a single square capillary tube. *Phys Rev Lett*. 2009;103(12):124502.
34. Yiotis AG, Salin D, Tajer ES, Yortsos YC. Drying in porous media with gravity-stabilized fronts: experimental results. *Phys Rev E*. 2012;86:026310.